JOURNAL OF CATALYSIS 150, 56–70 (1994)

# Surface Oxidation of Rhodium at Ambient Pressures as Probed by Surface-Enhanced Raman and X-Ray Photoelectron Spectroscopies

Anish A. Tolia,*,[1] R. J. Smiley,* W. N. Delgass,* Christos G. Takoudis,*,[1] and Michael J. Weaver†,[1]

*School of Chemical Engineering, Purdue University, West Lafayette, Indiana 47907-1283; and †Department of Chemistry, Purdue University, West Lafayette, Indiana 47907-1283

Received January 17, 1994; revised June 3, 1994

**Presented here is a comprehensive study of ambient-pressure thermal oxidation of rhodium surfaces utilizing surface-enhanced Raman spectroscopy (SERS) and X-ray photoelectron spectroscopy (XPS) as complementary techniques. Real-time SERS provides details regarding surface bonding and the time-dependent evolution of the surface oxides under *in situ* conditions, while XPS is used to obtain quantitative information about relative amounts of the oxides and extent of oxidation. The surfaces examined are electrochemically deposited rhodium thin films on gold substrates, and polycrystalline rhodium foil. Surface oxidation involved heating in a flowing stream of oxygen or oxygen/argon mixtures at atmospheric pressure, and temperatures up to 300°C. Raman spectra from the oxidized thin film exhibit several features in the 200–1000 $cm^{-1}$ region that may be attributed to rhodium–oxygen vibrations of surface oxygen and oxides. Bands at 530 and 800 $cm^{-1}$ are assigned to symmetric and asymmetric Rh–O stretches, respectively, in $Rh_2O_3$. A third band at 290 $cm^{-1}$, attributed to a Rh–O bending mode, arises from a behaviorally distinct oxide species. The corresponding XPS spectra exhibit several features that can be correlated with the SERS bands. The presence of $Rh_2O_3$ is inferred from the appearance of a Rh(3*d*) peak at 308.6 eV and a matching O(1*s*) peak at 530 eV. An additional O(1*s*) feature appears at 531.7 eV, which apparently correlates with the 290-$cm^{-1}$ SERS band. While a clearcut assignment of the latter has proven to be difficult, possible species are chemisorbed oxygen along with RhOOH or $RhO_2$. A differing reactivity of the spectrally distinct oxygen species towards CO was observed. A model for the spatial oxide composition is proposed based on a quantitative analysis of the XPS data.** © 1994 Academic Press, Inc.

## INTRODUCTION

Rhodium, as for other platinum-group transition metals, is a well-known catalyst for a wide variety of gas–solid catalytic reactions. Both the activity as well as the selectivity of rhodium catalysts are often found to be strongly dependent on the state of oxidation of the metal. For example, the presence of surface oxides is found to inhibit CO oxidation (1–3), while the activity for alkane hydrogenolysis, on the other hand, increases dramatically when the surface is oxidized (4, 5).

Oxygen adsorption on a variety of single-crystal Rh surfaces has been well documented. A number of studies in ultrahigh vacuum (UHV) have been reported on Rh(111) (6–9), Rh(100) (10), Rh(110) (11, 12), and on stepped rhodium surfaces (13). In a study of oxygen adsorption on polycrystalline rhodium, Campbell and White (14) reported formation of two types of oxygen having differing reactivities with carbon monoxide. The less reactive oxygen was attributed to a subsurface species. However, the aforementioned studies were limited chiefly to oxygen adsorption and did not involve elevated-temperature oxidation at substantial oxygen pressures to form either surface or bulk oxides. Among higher-pressure studies, Logan *et al.* (9) reported high-temperature oxidation of Rh(111) at oxygen pressures up to 80 Torr and reported oxides of stoichiometry Rh–O and $Rh_2O_3$, the formation of the latter being favored under more highly oxidizing conditions. Wong and McCabe (15) and Vis *et al.* (16) have reported changes in morphology of supported Rh crystallites during oxidation–reduction cycles, and report two different crystalline structures of $Rh_2O_3$. Ho and Yeh (17) gravimetrically examined oxygen chemisorption on Rh powders, obtaining a Rh/O ratio of 1 : 1 which they attribute to a monolayer of adsorbed oxygen. This ratio was found to increase at higher temperatures, from −50° to 25°C. Koshy (18) studied oxidation of thin Rh films on a NaCl substrate and found complete oxidation of 500 Å thick films, yielding $Rh_2O_3$ upon heating in air at 350°C.

The relative dearth of information on surface oxidation under realistic, catalytically relevant conditions arises in large measure from the lack of sensitive surface-analysis techniques applicable at higher gas pressures. A novel approach of this type involves the acquisition of vibrational spectra for metal–gas interfaces by using surface-enhanced Raman spectroscopy (SERS) (19–25). While

[1] Authors to whom correspondence should be addressed.



0021-9517/94 $6.00
Copyright © 1994 by Academic Press, Inc.
All rights of reproduction in any form reserved.

SERS is commonly considered to be limited to the coinage metals (Cu, Ag, Au), it can be readily extended to a range of other materials, including transition metals, by depositing them as thin films on SERS-active gold (22–28). While initial applications were to electrochemical interfaces (26, 27), we have found that this approach is particularly valuable for metal–gas interfaces since the residual gold sites tend to be inert towards adsorption and reactions such as gas-phase surface oxidation. Consequently, one has at hand an extremely sensitive technique for extracting vibrational information for interfacial species over a wide frequency range, including the low-frequency region (ca. 200–700 $cm^{-1}$) where surface–adsorbate (including metal–oxygen) vibrations are commonly located. In addition, this technique allows the acquisition of spectral sequences, even under atmospheric-pressure flow conditions, down to a timescale of seconds, enabling the evolution of processes such as surface oxidation to be studied under catalytically relevant conditions, including higher pressures and variable temperatures (24, 25).

A central, yet inadequately explored, issue in transition-metal surface oxidation concerns the stages in the process beyond initial oxygen chemisorption, especially the nature and structure of the oxides formed. Vibrational spectroscopy, especially if applied in a real-time mode under *in situ* conditions, can provide valuable information along these lines. Previous applications of surface vibrational spectroscopies to rhodium oxidation have been limited to electron energy-loss spectra (EELS) from single crystals in UHV (29, 30) and infrared and Raman spectra of thick oxide films or bulk-phase materials (31). Research from this laboratory has recently demonstrated the value of SERS for examining the oxidation of Pt, Rh, and Ru surfaces in aqueous electrochemical environments (28).

While such vibrational spectra yield valuable information on the nature of metal–oxygen bonding in surface oxidation, it is clearly desirable to obtain quantitative information on the extent of oxide formation and the nature of formal oxidation states. Although limited to UHV conditions, the technique of choice for such purposes is X-ray photoelectron spectroscopy (XPS). Oxidation of Rh has previously also been studied using XPS, encompassing single crystal Rh(111) (8, 32) and supported Rh catalysts (33–35). Many of these studies report an O(1*s*) peak at 530 eV for oxygen species associated with the rhodium. They also characterize the Rh(3*d*) chemical shift of ca. 2 eV due to oxidation from the 0 to +3 state. However, the O(1*s*) spectra from supported catalysts are of limited utility for characterizing states of oxygen due to the large O(1*s*) signal from the support.

We report here a detailed study of rhodium surface oxidation at atmospheric pressures and temperatures up to 300°C by using *in situ* SERS combined with XPS. These techniques provide complementary information concerning the structure and bonding of the rhodium oxides formed under these conditions.

## EXPERIMENTAL

The SERS-active Rh films were prepared as described elsewhere (22–25), utilizing 6-mm-diameter discs cut out of 0.1-mm-thick gold foil (Johnson Matthey), and polished using 0.3 $\mu$m alumina powder. They were then put into an electrode that exposed 3 mm of the surface and subjected to 25 oxidation–reduction cycles from −0.3 to 1.2 V vs SCE at 0.1 V $s^{-1}$ in 0.1 *M* KCl to produce the surface roughness necessary for Raman enhancement (36). The surface was rinsed thoroughly with deionized water and subsequently transferred to another cell for electrochemical deposition of the Rh overlayers. Rhodium was deposited from a 0.3-m*M* solution of $RhCl_3$ in 0.1 *M* $HClO_4$ at 0.1 V vs SCE and the cathodic charge was monitored and controlled in order to limit the deposition to the desired film thickness, usually less than 5 equivalent monolayers (27). Some XPS experiments were undertaken on a 0.1-mm-thick polycrystalline rhodium foil (Johnson Matthey).

The reactor utilized for the SERS experiments consists of a 300-ml 6-way cross which can be evacuated to $10^{-3}$ Torr by a mechanical pump (Edwards Model EM5). One of the arms of the cross contains an optical viewport over which the sample is mounted on an electrical feedthrough. The sample is welded to a tantalum foil to facilitate resistive heating. The sample can be heated to 350°C at atmospheric pressure and up to 600°C at reduced pressures. A chromel–alumel thermocouple spot welded between the Ta foil and the sample is used to monitor the temperature. Laser excitation is provided by a $Kr^+$ laser (Spectra Physics) at 647.1 nm. The scattered light is collected by a three-stage spectrometer (SPEX Triplemate) equipped with a Photometrics charge coupled device detector (CCD). The liquid-nitrogen-cooled CCD allows acquisition of real-time spectral sequences on a seconds timescale with a good signal-to-noise ratio. Gases are introduced into the reactor through a manifold that allows the mixing of up to four gases at a time. Gas flow rates are measured with a bubble flow meter. All gases used were of ultrahigh purity grade and obtained from Matheson Gases.

Most of the XPS experiments were performed on Rh films, deposited as described above on smooth gold foils. The foil (1.5 cm × 2.0 cm) completely covered the region of the molybdenum sample holder exposed to the X-ray source. All XPS experiments were performed on a Perkin-Elmer PHI 5300 XPS fitted with a PHI 04-800 catalytic reactor capable of heating samples to 600°C. Spectra were collected at a base pressure of about $10^{-9}$ Torr using an aluminum ($K_{\alpha 1,2}$ = 1486.6 eV) X-ray source operated at 15 kV and 400 W, an analyzer pass energy of 8.95 eV,

and with a channel-plate detector. The spectrometer was calibrated by setting the binding energies of the Au $4f_{7/2}$ and Cu $2p_{3/2}$ level values to 84.0 and 932.7 eV, respectively.

The XPS spectra were computer fit in order to determine the chemical state and quantity of specific species present on the samples. Curve fitting was carried out using a nonlinear least squares fitting program with a Gaussian/Lorentzian sum function. Rhodium metal was further fit with an exponential tail to account for its asymmetric character, arising because of core-hole coupling (37). The fitting routine constrained the area ratio for the spin-orbit split Rh($3d_{3/2,5/2}$) and Au($4f_{5/2,7/2}$) lines to 0.67 and 0.75, respectively. Intensities, peak positions, line widths, Gaussian/Lorentzian mix (fraction Gaussian), and exponential tail height and slope were all optimized by the fitting routine.

Some FTIR experiments were conducted on ca. 5 monolayers of rhodium electrochemically deposited on a 1 $cm^2$ gold foil in an *in situ* infrared reflection cell operated at atmospheric pressure. A Nicolet 800 spectrometer with a MCT-A type detector was used to acquire the spectra with 3000 scans at a resolution of 8 $cm^{-1}$. The detector was sensitive to frequencies down to 700 $cm^{-1}$. The sample compartment was purged with dry air to minimize interference from gas-phase water vapor. Morphological characterization of the Rh surfaces was performed by means of scanning tunneling microscopy (STM) in air. The microscope was a Nanoscope II (Digital Instruments), the STM tip was an electrochemically etched tungsten wire.

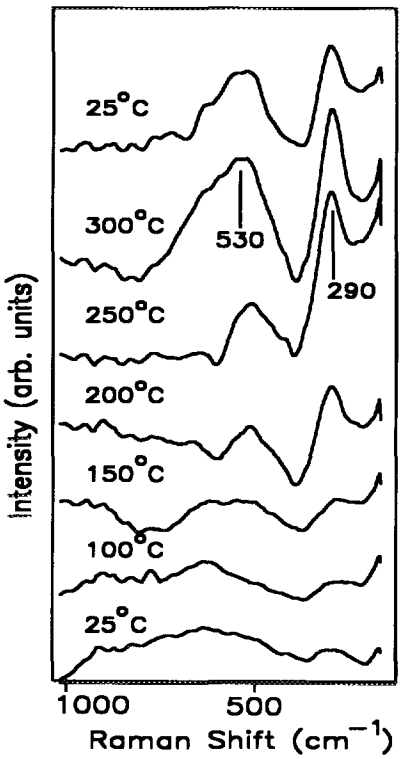


FIG. 1. Temperature-dependent SER spectra of a Rh thin film on roughened gold substrate exposed to a flowing mixture 150 cc/min of 30% $O_2$ in Ar at atmospheric pressure. The temperature was raised in increments of 50°C, holding at each temperature for ca. 2 min before stepping up to the next higher temperature. Integration time was 10 s.

## RESULTS

The composition and morphology of the electrochemically deposited rhodium film surfaces were characterized with scanning tunneling microscopy (STM), cyclic voltammetry, and scanning Auger electron spectroscopy (AES) in addition to XPS. STM micrographs of a gold surface roughened by electrochemical oxidation–reduction cycles to produce Raman enhancement showed lateral features of the order of 200 nm. This is consistent with literature reports of roughness features leading to good SERS enhancement (38). Deposition of 3–5 monolayers of rhodium resulted in some smoothing of these features. X-ray photoelectron spectra of the deposited overlayers yielded binding energies for the Rh($3d$) electrons identical to those obtained for a polycrystalline Rh foil, indicating that the rhodium film is not altered electronically by the underlying gold. Cyclic voltammograms obtained on these films in 0.1 *M* $HClO_4$ (27, 28) showed almost complete suppression of the gold oxidation and reduction waves, suggesting virtually complete coverage of the substrate by 3–5 equivalent monolayers of rhodium (cf. Ref. (27)). Scanning AES measurements also showed the film composition to be uniform on a 1-$\mu$m lateral scale, which is the resolution limit of the Auger spectrometer.

### *Surface Raman Spectroscopy*

The rhodium film surfaces were initially reduced by heating in a flowing mixture of 30% hydrogen in argon at ca. 150°C until the SERS background was free of metal–oxygen vibrational features in the 200–1000 $cm^{-1}$ region. Figure 1 shows typical spectra obtained while the sample was heated in a flowing mixture of 30% oxygen in argon in the following fashion: the temperature was raised from 25°C to 50°C and then to 300°C in steps of 50°C. About 1 min was needed for the temperature to reach the desired value, where it was maintained for ca. 2 min while spectra were acquired. This sequence resulted in Raman spectral features at 290 and 505 $cm^{-1}$ emerging at temperatures greater than 150°C (Fig. 1). Upon further heating the feature at 505 $cm^{-1}$ upshifted to 530 $cm^{-1}$ and became broader. No other bands were observed in the low-frequency (200–1000 $cm^{-1}$) region upon heating to 350°C. The 290 and 530 $cm^{-1}$ Raman bands increased in intensity with increasing sample temperature, and remained unaltered upon cooling the surface subsequently

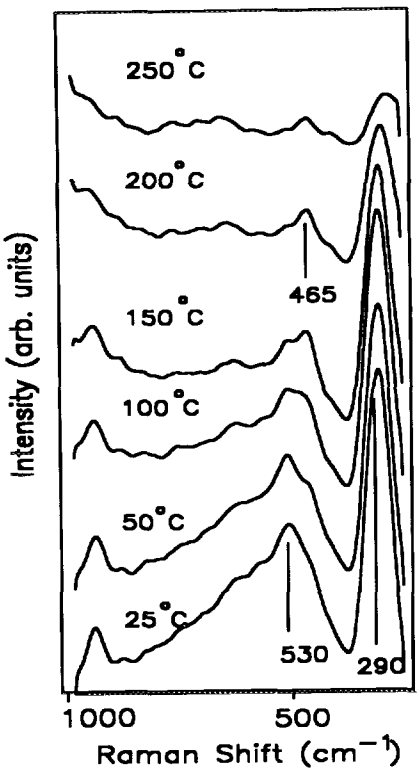


FIG. 2. Temperature-dependent SER spectra of an oxidized Rh surface exposed to a flowing gas mixture of 150 cc/min of 20% CO in Ar at atmospheric pressure. Other details as in Fig. 1.

to room temperature and evacuation of the reactor. Removal of these features required heating the surface in 30% hydrogen in argon to 200°C.

In order to assist elucidating the nature of, and possible relationship between, the oxygen species responsible for the two vibrational bands, the reactivity of such oxidized Rh surfaces with CO was examined. A Rh surface, oxidized in the temperature-programmed manner described above, was exposed to a flowing stream of 20% CO in Ar. Representative SER spectra obtained during such an experiment are presented in Fig. 2. There is no attenuation of the peak at 290 $cm^{-1}$ evident at temperatures below 150°C, while the feature at 530 $cm^{-1}$ shows some decrease in intensity. At temperatures higher than 100°C, there is evidence of adsorbed CO in the form of the Raman peak at 465 $cm^{-1}$ assigned to the Rh–CO stretch of adsorbed CO (22, 24, 25). At temperatures above 150°C, both the 290- and 530-$cm^{-1}$ features are removed by CO, although the latter disappears at a lower temperature (Fig. 2). The two Raman bands therefore appear to arise at least partially from two different kinds of oxygen or oxide species rather than from different vibrational modes within a uniform structure. Nonetheless, reducing the oxidized rhodium surface with hydrogen in the same fashion yielded simultaneous temperature-dependent attenuation of both the 290- and 530-$cm^{-1}$ features.

The effect of varying the temperature-time profile on the formation of the oxide vibrational bands was also studied. Rhodium surfaces were exposed, as before, to 150 cc/min of 30% oxygen in argon. A series of experiments was performed which involved heating a previously reduced surface in fast (ca. 1 min) temperature steps, recording spectra at a given temperature every 30 s, and cooling down to room temperature (requiring ca. 1 min) before stepping up to the next higher temperature. Figure 3 shows typical results of these experiments. Interestingly, when the temperature was stepped to 150°C (Fig. 3A), only the 290 $cm^{-1}$ feature was observed. When the temperature was then stepped to 200°C (Fig. 3B), the 530 $cm^{-1}$ band began to appear after about 7 min. When the temperature was subsequently stepped to 250°C (Fig. 3C), the 290 $cm^{-1}$ feature disappeared in about 3 min, the band at 530 $cm^{-1}$ increased in intensity and another feature at 800 $cm^{-1}$ appeared. The SERS band at ca. 920 $cm^{-1}$ arises from a background feature on the gold substrate. Such features are sometimes visible due to the presence of "pinholes" in the Rh film. Further heating of the surface intensified these bands but resulted in no new features.

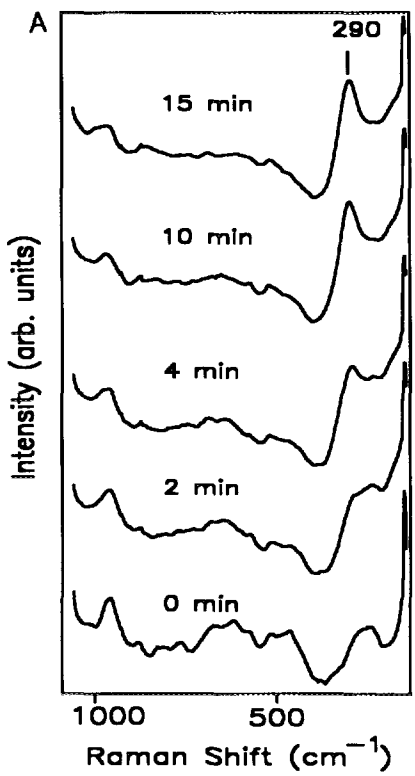


FIG. 3A. Real-time SER spectra of an initially reduced Rh surface subjected to a fast temperature step to 150°C in a flowing mixture of 150 cc/min of 30% $O_2$ in Ar. Data were collected every 30 s, but only selected spectra are shown for clarity. Integration time was 10 s.

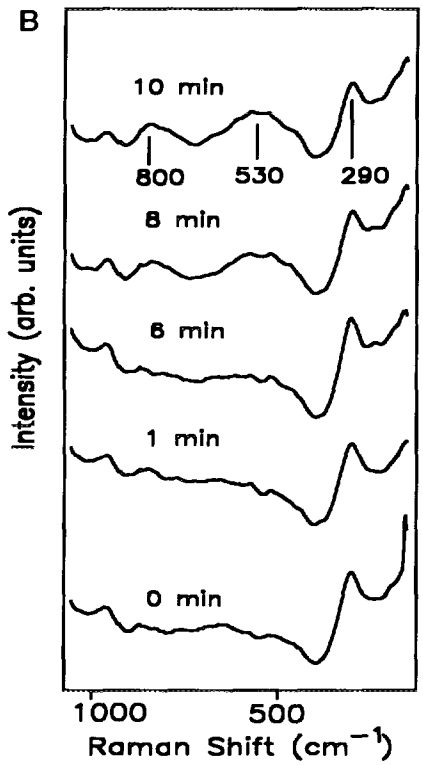


FIG. 3B. Real-time SER spectra of a Rh surface subjected to a fast temperature step to 200°C. The surface had been previously subjected to treatment described in Fig. 3A, and subsequently cooled to room temperature. Other details as in Fig. 3A.

Heating an initially reduced surface rapidly to relatively high temperatures yielded somewhat different results, as shown in Fig. 4. When a reduced surface was heated rapidly to 200°C, the 290 $cm^{-1}$ feature appeared as a transient and disappeared within 2–3 min. The band at 530 $cm^{-1}$ appeared within 1 min of the temperature step, but was broad and highly asymmetric. After about 3 min, a band at 800 $cm^{-1}$ appeared; at the same time the 530 $cm^{-1}$ feature narrowed, became more symmetric, and upshifted to about 550 $cm^{-1}$. The change in symmetry of the broad band at ca. 530 $cm^{-1}$ is synchronous with the disappearance of the 290 $cm^{-1}$ feature. When a reduced surface was subjected to a temperature step of 300°C, only the 530- and 800-$cm^{-1}$ features were observed; the 290-$cm^{-1}$ band was not even transiently observed (at 30 s intervals). Note that the top spectrum in Fig. 4 shows for comparison a 200–1000 $cm^{-1}$ segment of a normal Raman spectrum for bulk-phase $Rh_2O_3$ (Strem Chemicals), obtained using the same excitation wavelength of 647.1 nm. Evident is a similarity of the 530-$cm^{-1}$ feature for this compound with the 530 $cm^{-1}$ SERS band.

Some SERS experiments were performed with rhodium films having different thicknesses, adjusted by appropriate alterations in the electrodeposition time. In sharp contrast to the behavior of thicker films, oxidation of Rh films less than two equivalent monolayers thick resulted in the *exclusive* formation of the feature at 290 $cm^{-1}$, under all temperature and heating conditions used.

Attempts were also made to examine the higher frequency spectral region, including the 3500-$cm^{-1}$ region where other oxygen species such as surface hydroxyls exhibit vibrational features. However, detector sensitivity and signal-to-noise limitations prevented conclusive identification of any spectral features in this region. In an attempt to overcome this limitation, $H_2$ was replaced by $D_2$ for the initial reduction step, but subsequent oxidation did not lead to any discernable bands in the O–D stretch (ca. 2600 $cm^{-1}$) region.

### *X-Ray Photoelectron Spectroscopy*

The corresponding XPS experiments were performed primarily on rhodium films deposited on smooth gold foils. Experiments were also repeated with a roughened gold foil and approximately the same rhodium coverage. Such results showed no significant deviation from the ones with a smooth foil. The rhodium films were initially reduced by heating in hydrogen at 300°C for 4 h and subsequently

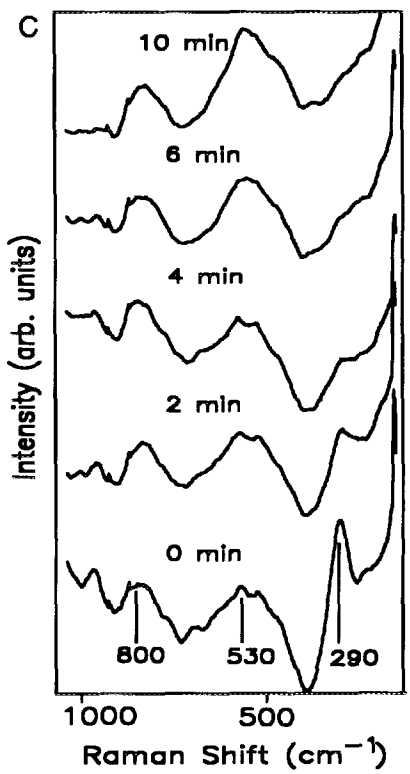


FIG. 3C. Real-time SER spectra of a Rh surface subjected to a fast temperature step to 250°C. The surface had been previously subjected to treatment described in Figs. 3A and 3B, and subsequently cooled to room temperature. Other details as in Fig. 3A.

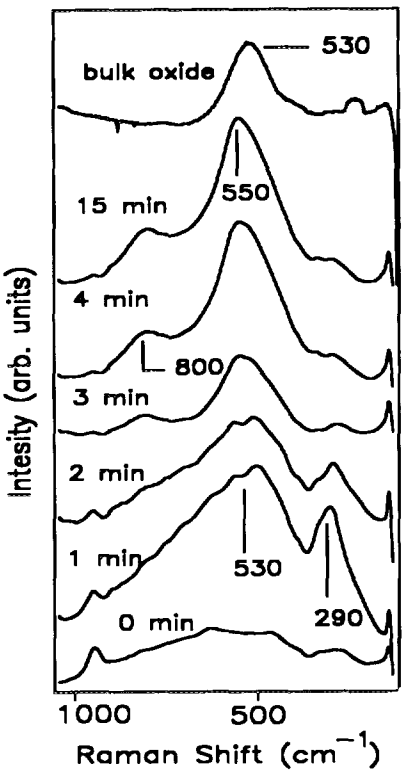


FIG. 4. Real-time SER spectra of an initially reduced Rh surface subjected to a fast temperature step to 200°C in a flowing mixture of 150 cc/min of 30% $O_2$ in Ar. Spectra were collected every 30 s, but only selected members of the sequence are shown for clarity. Normal Raman spectrum of bulk $Rh_2O_3$ is included for comparison. Integration time was 10 s.

oxidized by heating in oxygen at a sequence of progressively higher temperatures, in increments of 50°C up to 300°C (as for the corresponding SER spectra, *vide supra*), for 30 min each time. For each temperature, the heating rate was 3°C min$^{-1}$ with a gas-flow rate of 30 cc/min. To ensure complete oxidation, samples were eventually heated in oxygen at 300°C for 12 h. After each stage of oxidation, the sample was cooled to ambient temperatures and transferred, without exposure to air, from the reactor to the main UHV chamber for analysis.

Figure 5 shows curve-fit Rh(3*d*), O(1*s*) and C(1*s*) XPS spectra obtained for the stepwise oxidation of a rhodium film surface. The top spectrum (a) refers to the initially reduced surface; (b)–(e) are representative members of the spectral sequence obtained following oxidation at progressively higher temperatures up to 300°C. Table 1 summarizes the best-fit parameters obtained from these data and includes the peak positions, integrated areas, area percentages, and line widths. In addition, Table 1 shows the peak splitting of the Rh $3d_{5/2,3/2}$ and Au $4f_{7/2,5/2}$, as well as the exponential tail height and slope for the $Rh^0$ species.

The fully reduced rhodium film yields an asymmetric $3d_{5/2}$ peak at 307.3 eV and a spin-orbit splitting of 4.7 eV. At temperatures above 50°C, the Rh(3*d*) spectra show a noticeable shoulder at ca. 308.5 eV. This higher binding energy is consistent with values reported in the literature for $Rh^{3+}$ in $Rh_2O_3$ (8, 32–35). The extent of rhodium oxidation, as gauged by the intensity of the emerging 308.6 eV peak relative to the 307.3 eV feature, is seen to increase roughly linearly with temperature. Most of the rhodium was found to be converted to $Rh^{3+}$ after the 30 min of exposure to oxygen at 300°C in the temperature sequence, and there was no evidence of any $Rh^0$ remaining after an additional 12 h of oxygen exposure at 300°C. The initial spectrum (a) in the O(1*s*) region displays a weak band at 532 eV, probably arising from adsorbed water. Upon heating the sample, a broad peak appears initially at about 531 eV, which is probably due to at least two distinct species. At the end of the heating cycle, two distinct peaks are evident at 530 and 531.7 eV. Fits of the overlapping features are included with the temperature-dependent O(1*s*) spectra in Fig. 5 and described quantitatively in Table 1.

The C(1*s*) spectra were also collected in order to account for any oxygen associated with carbon-containing surface species. They exhibit a large peak centered at 284.5 eV, assigned to aliphatic and amorphous carbon, and a shoulder at higher binding energy. The shoulder may be resolved into three peaks shifted from the main peak by approximately 1.5, 3, and 4 eV, which correspond, respectively, to alcohol and/or ether, carbonyl, and carboxyl chemical states (39). The amount of oxidized carbon increases steadily until about 150°C and then quickly decreases as the carbon is burned off the surface. The total oxygen-to-rhodium ratio under fully oxidized conditions accounting for all the oxygen except that associated with carbon is about 2.5 : 1. This approximate atomic ratio was calculated by normalizing each peak area by the photoemission cross section computed by Scofield (40).

Analogous to the SERS experiments, the reactivity of oxidized Rh surfaces with CO was also investigated with XPS. The oxidized rhodium film was heated in CO at increasing temperatures up to 300°C for 30 min at each temperature. Finally, the surface was maintained at a temperature of 300°C in CO for 12 h. Figure 6 shows the Rh(3*d*), O(1*s*), and C(1*s*) XPS spectra and Table 2 summarizes corresponding curve-fitting results for the CO reduction of oxidized rhodium on gold. Exposure to CO at 35°C yields partial reduction of the $Rh^{3+}$. Reduction at temperatures greater than 200°C results in complete replacement of the 308.6 eV peak by one at 307.3 eV, as shown in Fig. 6. Corresponding changes are also seen in O(1*s*) spectra as indicated by the attenuation of the oxygen features. All oxygen present on the surface at temperatures ≥200°C can be associated with surface carbon and

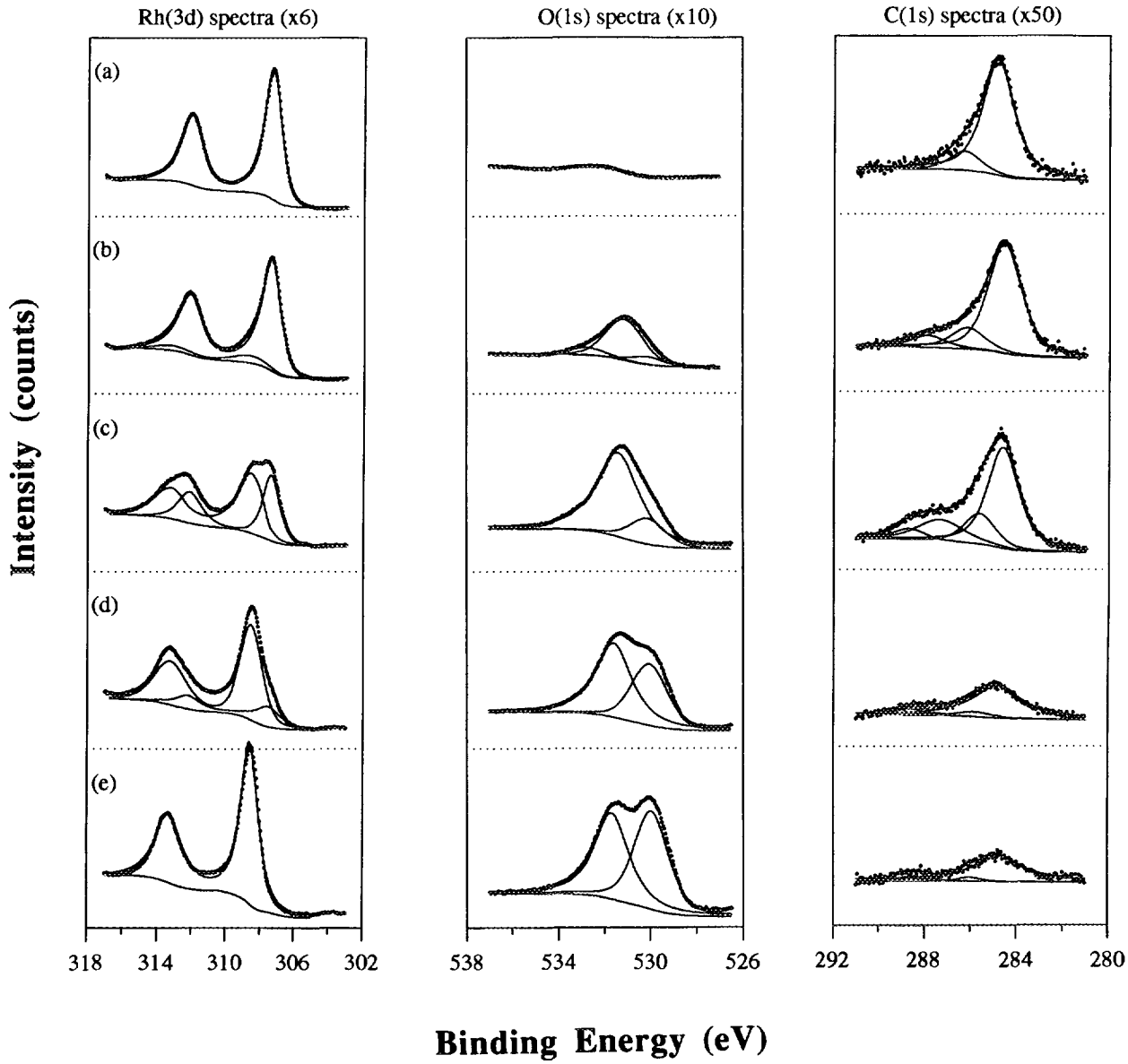


FIG. 5. Rh(3*d*), O(1*s*), and C(1*s*) XPS spectra for oxidation of a rhodium thin film deposited on a smooth gold substrate. Sample initially reduced in $H_2$ at 300°C for 4 h (a), and then oxidized in $O_2$ for 30 min at 50°C (b), 150°C (c), 250°C (d), and 300°C for 12 h (e).

is fit with one peak. At lower temperatures, however, the oxygen signal includes not only the contributions from oxidized carbon but also a substantial quantity of additional oxygen associated with the rhodium, manifested in the O(1*s*) peaks at 530 and 531.7 eV. As shown in Fig. 7, even temperatures as low as 35°C appear to be sufficient to initiate the removal of the oxygen peak at 530 eV. Noticeable attenuation of the peak at 531.7 eV requires temperatures of at least 100°C, after which both O(1*s*) peaks show significant decrease in intensity with increasing temperature. C(1*s*) spectra show a substantial increase in carbon content on the surface with increasing temperature in CO. The increase in carbon at 284.5 eV can be explained by disproportionation of CO on the rhodium surface. In addition, these spectra show an increase in the peak at ca 286 eV with increasing reduction temperature, which is due to the adsorption of CO onto the sample, and reveal that this peak goes through a maximum at about 200°C before decreasing at higher temperatures.

Also, similar to the Raman experiments, oxidation of rhodium thin films less than two equivalent monolayers thick was examined with XPS. In this case, although both the 530 eV and the 531.7 eV O(1*s*) peaks were observed, the peak at 530 eV was diminished relative to that at 531.7,

TABLE 1

**Fitted Parameters for O(1*s*), Rh(3*d*), C(1*s*), and Au(4*f*) Spectra for Oxidation of Rhodium Film[a]**

| Temp (°C)[b]: | | 50 | 150 | 250 | 300 |
|---|---|---|---|---|---|
| Oxid. time (h): | 0[c] | 0.5 | 0.5 | 0.5 | 12 |
| | | *O(1s)* | | | |
| BE (eV)[d] | | 530.1 | 530.1 | 530.0 | 530.0 |
| FWHM (eV) | | 1.5 | 1.8 | 1.8 | 1.7 |
| % AREA | | 12.5 | 17.7 | 39.7 | 50.0 |
| BE (eV) | | 531.1 | 531.4 | 531.6 | 531.7 |
| FWHM (eV) | | 1.9 | 2.1 | 1.8 | 1.7 |
| % AREA | | 73.7 | 82.3 | 60.3 | 50.0 |
| BE (eV) | 532.3 | 532.7 | | | |
| FWHM (eV) | 2.5 | 2.0 | | | |
| % AREA | 100.0 | 13.8 | | | |
| Total area ($10^{-3}$) (counts eV) | 2.8 | 14.5 | 30.5 | 41.1 | 53.6 |
| | | *Rh(3d)* | | | |
| BE ($3d_{5/2}$) (eV) | 307.3 | 307.3 | 307.3 | 307.5 | |
| FWHM (eV) | 1.2 | 1.2 | 1.2 | 1.8 | |
| S.O. split (eV)[e] | 4.7 | 4.7 | 4.7 | 4.6 | |
| TAIL height[f] | 0.2 | 0.4 | 0.6 | 0.7 | |
| TAIL slope[f] | 0.4 | 0.3 | 0.4 | 0.5 | |
| % AREA | 100.0 | 89.4 | 62.9 | 14.5 | |
| BE ($3d_{5/2}$) (eV) | | 308.6 | 308.5 | 308.5 | 308.6 |
| FWHM (eV) | | 2.3 | 1.7 | 1.5 | 1.2 |
| S.O. split (eV) | | 4.5 | 4.6 | 4.7 | 4.7 |
| % AREA | | 10.6 | 37.1 | 85.5 | 100.0 |
| Total area ($10^{-3}$) (counts eV) | 78.0 | 69.3 | 59.3 | 69.9 | 97.5 |
| | | *C(1s)* | | | |
| BE (eV) | 284.5 | 284.5 | 284.5 | 284.8 | 284.8 |
| FWHM (eV) | 1.6 | 1.7 | 1.6 | 2.5 | 2.4 |
| % AREA | 86.7 | 75.7 | 58.7 | 80.2 | 85.4 |
| BE (eV) | 286.2 | 286.1 | 285.7 | 285.8 | 286.0 |
| FWHM (eV) | 1.6 | 1.7 | 1.6 | 1.7 | 1.1 |
| % AREA | 13.3 | 15.5 | 17.0 | 7.4 | 4.5 |
| BE (eV) | | 287.8 | 287.3 | 287.6 | |
| FWHM (eV) | | 1.7 | 2.3 | 1.3 | |
| % AREA | | 8.8 | 18.0 | 3.5 | |
| BE (eV) | | | 288.6 | 288.6 | 288.5 |
| FWHM (eV) | | | 1.6 | 1.6 | 1.5 |
| % AREA | | | 6.4 | 8.9 | 10.1 |
| Total area ($10^{-3}$) (counts eV) | 8.1 | 7.7 | 7.3 | 3.9 | 3.2 |
| | | *Au(4f)*[g] | | | |
| Total area ($10^{-3}$) (counts eV) | 597.0 | 525.0 | 422.0 | 547.0 | 557.0 |

[a] Curve-fit data from Fig. 5.
[b] Temperature at which oxidation of surface (in 1 atm $O_2$) proceeds, for incremental time periods indicated (see text). Only representative members of temperature-dependent data given; spectra were obtained in 50°C increments (see text).
[c] Data in this column obtained for initially reduced surface.
[d] Binding energy.
[e] Spin–orbit splitting.
[f] Parameters used to fit an exponential tail to the data in order to account for asymmetry in line shape arising from core–hole coupling. The tail height and slope control the maximum value and high energy decay rate of the asymmetric tail function applied for energies higher than $E_0$.
[g] BE ($4f_{7/2}$) = 84.0 eV, FWHM = 1.1 eV, S.O. Split = 3.7 eV.

when compared with data obtained during the oxidation of thicker (3–5 monolayer) rhodium films.

To determine whether the thin films of rhodium on gold behave analogously to metallic rhodium, and to establish the effects of structural changes in the film, the oxidation–reduction treatments were repeated on a polycrystalline Rh foil and examined with XPS. Oxidation of the foil resulted in XPS peaks similar to those obtained during oxidation of the thin films, with slightly higher O(1*s*) intensities observed at 531.7 eV versus 530 eV for the foil. As expected, oxidation under conditions identical to those used for the thin films did not result in complete oxidation of the 0.1-mm-thick foil, and the Rh(3*d*) line showed evidence of metallic rhodium during the entire oxidation–reduction cycle. Reaction of the 530 and 531.7 eV oxygen species with CO also resulted in behavior similar to that observed previously, with the O(1*s*) peak at 530 eV again being selectively reduced at lower temperatures.

Additional insight concerning the depth distribution for the oxidized rhodium oxides was gained from angle-resolved XPS (ARXPS) analysis of the polycrystalline rhodium foil, following oxidation at 300°C for 4 h. This analysis for the foil sample is considerably less complex when compared to the thin rhodium film because the former surface is relatively flat, and the oxide layer can be assumed to be fairly uniform. By lowering the electron take-off angle with respect to the sample surface, surface species are enhanced while bulk ones are attenuated (41, 42). ARXPS results, collected at 25°, 45°, and 75°, with respect to the surface plane, using a magnesium X-ray source, are shown in Fig. 8 and clearly show the surface enhancement at low angles of the $Rh^{3+}$ compared to $Rh^0$. The O(1*s*) spectra show three features, including the previously observed peaks, 530 eV, ca. 531.7 eV, and an additional one at 533.5 eV. The 531.7-eV peak is enhanced at lower angles compared to the other two oxygen bands. The presence of the higher binding energy peak at 533.5 eV is confirmed by heating the sample *in situ* to 300°C in the XPS main chamber. The corresponding temperature-dependent spectral sequence is shown in Fig. 9. At temperatures above 200°C, the lower binding energy peaks are no longer evident, leaving behind only the 533.5-eV feature.

### *Infrared and STM Characterization*

In order to identify surface vibrational features in the high frequency (>3000 $cm^{-1}$) region, which is not as readily accessible with SERS (given our present detector response characteristics), the oxidized rhodium films were also examined with infrared reflection-absorption spectroscopy (IRAS). These experiments were motivated by the possible presence of surface hydroxyl species (*vide infra*). The infrared spectra were obtained *in situ* at atmo-

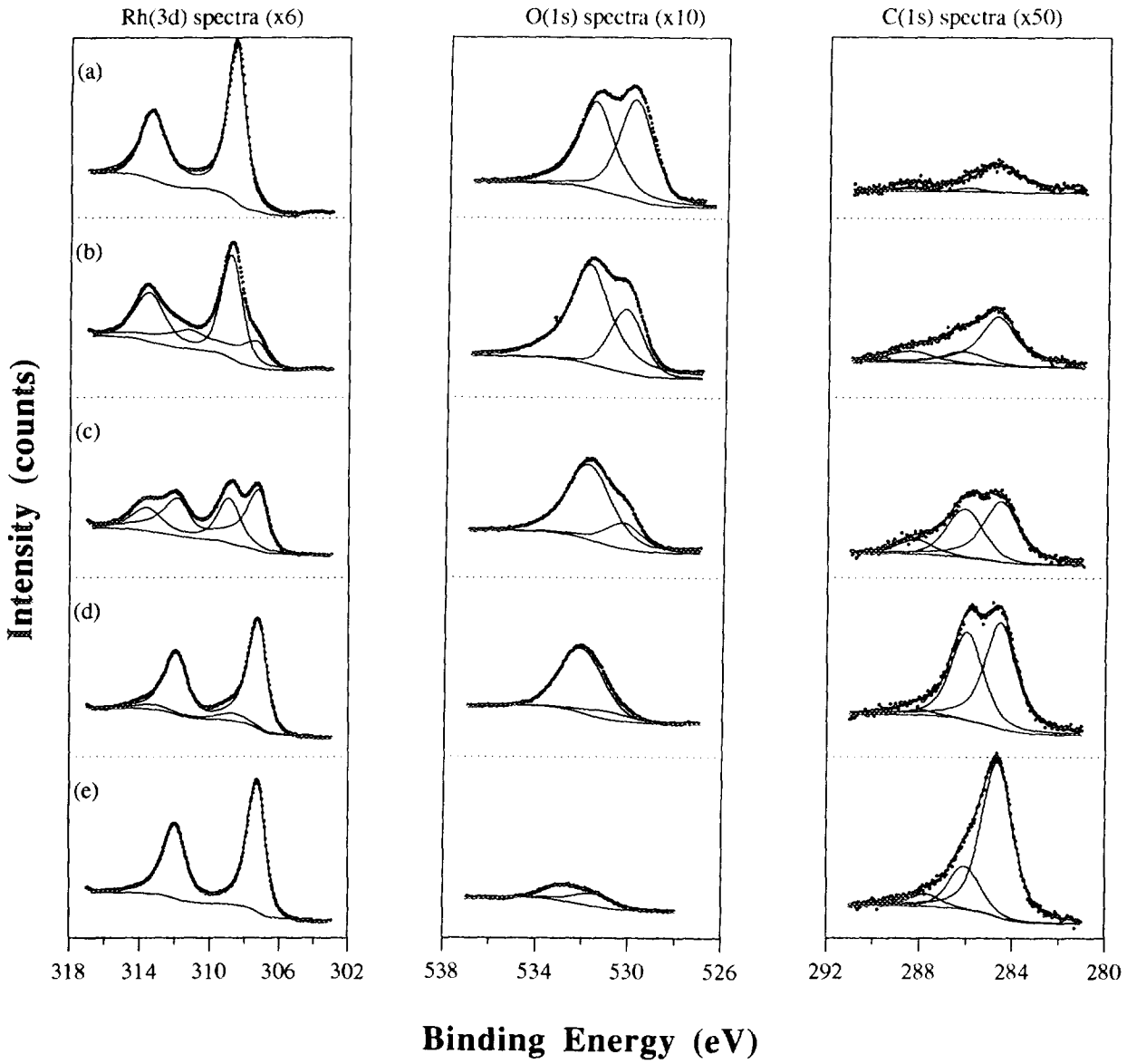


FIG. 6. Rh(3*d*), O(1*s*), and C(1*s*) XPS spectra for reduction of a rhodium thin film deposited on a smooth gold substrate by CO. Sample oxidized by heating in $O_2$ to 300°C for 12 h (a), and then reduced in CO for 30 min at 50°C (b), 100°C (c), 150°C (d), and then 300°C for 12 additional h (e).

spheric pressure in a catalytic reactor. Samples were initially reduced in hydrogen at 300°C for 2 h, and subsequently oxidized in oxygen at 300°C for 30 min. The reactor was evacuated and purged with nitrogen between the reduction and oxidation steps. The spectra obtained for the reduced surface were used as the IRAS reference, and both *s*- and *p*-polarized spectra were collected to minimize the effects of gas-phase interference. These experiments did not reveal any features in the 3000–3700 $cm^{-1}$ region that could be attributed to surface species.

The structural changes imposed on the rhodium thin film by oxidation were also studied briefly with scanning tunneling microscopy (STM). Micrographs were obtained at each stage of the sample preparation: roughened gold substrate, substrate with deposited rhodium thin film and films oxidized by heating in oxygen at 300°C for 30 min. In addition to the characterization of the substrate and deposited films, the analysis showed that oxidation of the film caused the surface to break up into smaller structures.

## DISCUSSION

Both the SERS and XPS spectra gathered for the oxidized rhodium films indicate the presence of at least two

TABLE 2

**Fitted Parameters for O(1s), Rh(3d), C(1s), and Au(4f) Spectra for Reduction of Rhodium Film by CO[a]**

| Temp (°C)[b]: | | 50 | 100 | 150 | 300 |
|---|---|---|---|---|---|
| Red. time (h): | 0[c] | 0.5 | 0.5 | 0.5 | 12 |
| | | O(1s) | | | |
| BE (eV)[d] | 530.0 | 530.3 | 530.3 | 530.9 | |
| FWHM (eV) | 1.7 | 1.7 | 1.9 | 2.2 | |
| % AREA | 50.0 | 28.6 | 22.5 | 11.0 | |
| BE (eV) | 531.7 | 531.8 | 531.8 | 532.0 | 532.3 |
| FWHM (eV) | 1.7 | 2.0 | 2.1 | 2.2 | 2.7 |
| % AREA | 50.0 | 71.4 | 77.5 | 89.0 | 100.0 |
| % AREA[e] | 45.6 | 51.3 | 42.4 | 25.7 | 0 |
| Total area ($10^{-3}$) (counts eV) | 53.6 | 51.8 | 37.0 | 22.6 | 7.8 |
| | | Rh(3d) | | | |
| BE ($3d_{5/2}$) (eV) | | 307.3 | 307.2 | 307.2 | 307.2 |
| FWHM (eV) | | 1.4 | 1.2 | 1.2 | 1.2 |
| S.O. split (eV)[f] | | 4.0 | 4.6 | 4.7 | 4.7 |
| TAIL height[g] | | 0.7 | 0.6 | 0.4 | 0.3 |
| TAIL slope[g] | | 0.5 | 0.4 | 0.3 | 0.4 |
| % AREA | | 30.0 | 57.4 | 88.8 | 100.0 |
| BE ($3d_{5/2}$) (eV) | 308.6 | 308.7 | 308.8 | 308.6 | |
| FWHM (eV) | 1.2 | 1.4 | 1.5 | 2.0 | |
| S.O. split (eV) | 4.7 | 4.7 | 4.7 | 4.7 | |
| % AREA | 100.0 | 70.0 | 42.6 | 11.2 | |
| Total area ($10^{-3}$) (counts eV) | 97.6 | 86.7 | 80.6 | 67.7 | 80.6 |
| | | C(1s) | | | |
| BE (eV) | 284.8 | 284.7 | 284.6 | 284.5 | 284.6 |
| FWHM (eV) | 2.4 | 1.9 | 1.8 | 1.6 | 1.5 |
| % AREA | 85.4 | 55.1 | 52.8 | 54.8 | 74.9 |
| BE (eV) | 286.0 | 286.2 | 286.1 | 285.9 | 286.0 |
| FWHM (eV) | 1.1 | 2.1 | 1.8 | 1.6 | 1.5 |
| % AREA | 4.5 | 31.4 | 36.4 | 42.6 | 19.5 |
| BE (eV) | | | | 288.0 | 287.7 |
| FWHM (eV) | | | | 1.6 | 1.5 |
| % AREA | | | | 2.6 | 5.6 |
| BE (eV) | 288.5 | 288.5 | 288.2 | | |
| FWHM (eV) | 1.5 | 2.3 | 1.8 | | |
| % AREA | 10.1 | 13.4 | 10.8 | | |
| Total area ($10^{-3}$) (counts eV) | 3.2 | 6.1 | 7.6 | 10.8 | 11.5 |
| | | Au(4f)[h] | | | |
| Total area ($10^{-3}$) (counts eV) | 557.0 | 525.0 | 566.0 | 533.0 | 588.0 |

[a] Curve-fit data from Fig. 6.

[b] Temperature at which CO reduction (in 1 atm) proceeds, for incremental time periods indicated (see text).

[c] Data in this column obtained for initially oxidized surface.

[d] Binding energy.

[e] Area percentage for O(1s) 531.7 eV peak after correction for oxygen associated with carbon. Assumes an oxygen to carbon ratio of 2:1 for oxygen associated with carbon at a binding energy of ca. 288.5, and a oxygen to carbon ratio of 1:1 for oxygen associated with carbon at binding energies of ca. 286.0 eV and 287.8 eV. Calculations have accounted for differences in Scofield cross sections for O(1s) and C(1s) electrons.

[f] Spin–orbit splitting.

[g] Parameters used to fit an exponential tail to the data as in Table 1.

[h] BE ($4f_{7/2}$) = 84.0 eV, FWHM = 1.1 eV, S.O. split = 3.7 eV.

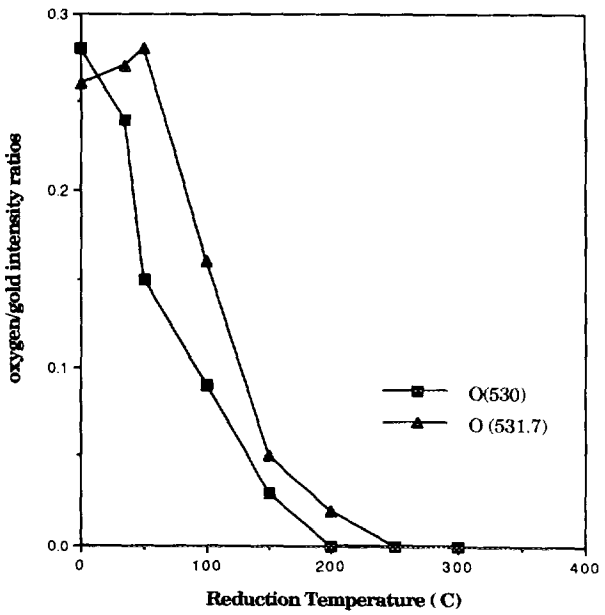


FIG. 7. Changes in individual oxygen peaks at 530- and 531.7-eV (corrected by subtracting oxygen associated with surface carbon) area ratios as a function of CO reduction temperature.

forms of chemisorbed oxygen or oxide. This finding is deduced primarily from the appearance of behaviorally distinct metal–oxygen ($\nu_{M-O}$) vibrational bands at 530 and 290 $cm^{-1}$, and oxygen (1s) binding energies at 530 and 531.7 eV. Moreover, there is consistent evidence derived from the conditions required for their formation, and their

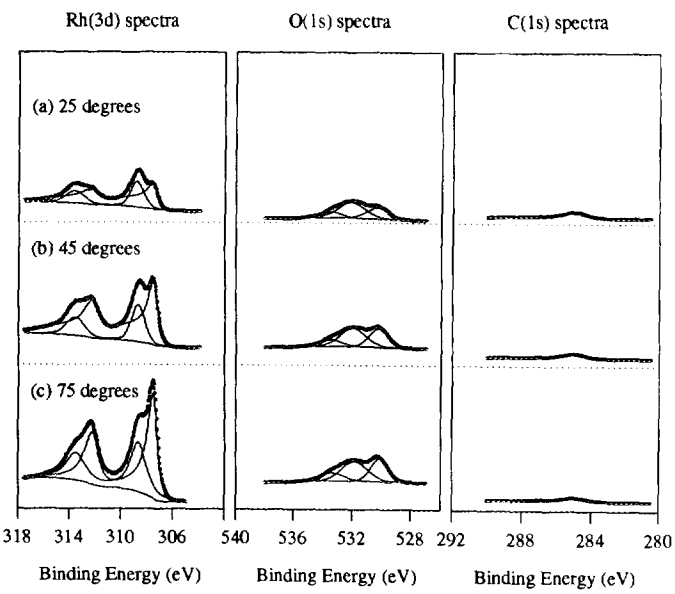


FIG. 8. Rh(3d), O(1s), and C(1s) angle-resolved XPS spectra of a Rh foil initially reduced in hydrogen at 300°C for 4 h and then heated in oxygen at 300°C for 4 h.

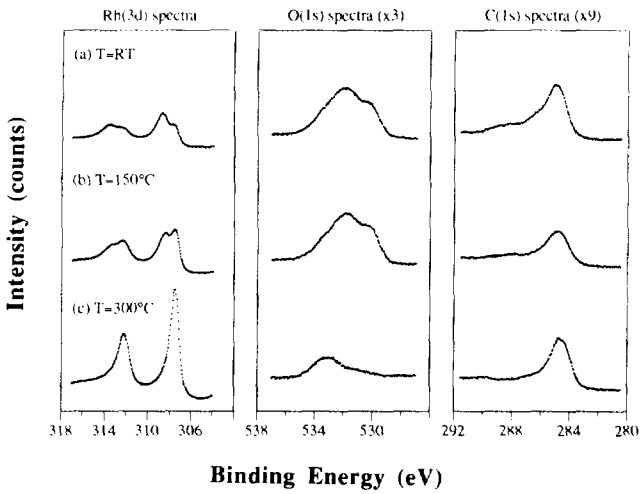


FIG. 9. Rh(3*d*), O(1*s*), and C(1*s*) spectra for decomposition of the rhodium oxides. An oxidized rhodium foil was heated *in situ* in the UHV chamber, and spectra were collected after 3 h intervals at the temperatures indicated.

differing reactivity with CO, to suggest that the 530 $cm^{-1}$ vibrational band arises from the species manifested in the XPS as the 530 eV peak. Both these features are predominant on thicker rhodium films oxidized at high temperatures (>250°C), and both are attenuated preferentially upon reduction with CO.

We assign these features to a rhodium oxide, $Rh_2O_3$. Several lines of evidence support this assertion. The XPS O(1*s*) binding energy, 530 eV, is indicative of an oxidic oxygen, and the corresponding Rh(3*d*) peak at 308.6 eV is consistent with the presence of $Rh^{3+}$ (8, 32–35). While complicated by the involvement of the additional O(1*s*) features, the Rh–O stoichiometry inferred from XPS (*vide infra*) is also suggestive of $Rh_2O_3$. As mentioned above, this species is known (or anticipated) to be formed upon extensive rhodium oxidation (9, 15–18, 32–35). The similarity of the normal Raman 530 $cm^{-1}$ band for $Rh_2O_3$ (Fig. 4) with the corresponding SERS feature for extensively oxidized rhodium supports the assignment of the latter to an Rh–O stretching mode for strongly oxidized rhodium, most probably $Rh_2O_3$. The weak SERS band at 800 $cm^{-1}$ also seen under these conditions most likely arises from another lattice mode for the same species: comparison with spectra for transition metal–oxo complexes (43) suggests that the band is due to an asymmetric stretch for Rh–O–Rh.

The observed virtual absence of the 530-$cm^{-1}$ SERS feature for strongly oxidized rhodium films thinner than about two equivalent monolayers indicates that the full development of the $Rh_2O_3$ structure requires multilayer oxide growth. This finding, although perhaps unsurprising since the integrity of a true stoichiometric oxide would seemingly demand a three-dimensional structure, is noteworthy inasmuch as it highlights the virtues of utilizing thin metal films to interrogate such spatial effects.

A more unexpected feature of the present results is the appearance of an additional, behaviorally distinct, oxygen species upon rhodium oxidation as manifested by the SERS band at 290 $cm^{-1}$ and the XPS peak at 531.7 eV. As for the 530-$cm^{-1}$/530-eV pair, the 290-$cm^{-1}$/531.7-eV SERS/XPS features also appear to be associated with the same type of surface oxygen moiety. This latter deduction, although less firm than the former, is derived primarily from the consistent correlation established between the appearance of the 290-$cm^{-1}$ SERS and 531.7-eV features upon temperature-programmed oxidation, their dominance for oxidized ultrathin (<2 equivalent monolayer) Rh films, and their apparent resistance to reductive removal by CO.

The identity of the oxygen moiety responsible for these spectral features has proved to be difficult to establish. The low frequency of the 290-$cm^{-1}$ SERS band suggests an assignment involving a Rh–O bending, rather than stretching, vibration (43). The relatively high O(1*s*) binding energy of the 531.7-eV XPS feature is indicative of a less electron-rich oxygen, as might be anticipated for chemisorbed oxygen (rather than a bona fide oxide), a hydroxyl, or possibly another type of oxide oxygen. Further evidence favoring particular assignments, as well as an assay of the amount of surface oxygen species produced, can be extracted from quantitative analysis of the XPS data, including the angle-dependent spectra. This analysis was undertaken as follows.

Given that the present system inevitably involves multilayer oxidation, it is necessary to utilize an analysis which accounts for the differing mean-free paths of the escaping core electrons, $\lambda_i$, in a presumed matrix material. The necessary $\lambda_i$ values were determined using the procedure of Tanuma *et al.* (44); these are summarized in Table 3. Note that since an Al X-ray source was used for the

TABLE 3

**Calculated Inelastic Mean-Free Path of Electrons, $\lambda[i, j]$ for Core Electron, *i*, in Matrix Material, *j***

| | Al anode (Å) | Mg anode (Å) |
|---|---|---|
| $\lambda$[O(1*s*), O] | 16.51 | 13.40 |
| $\lambda$[O(1*s*), $Rh_2O_3$] | 16.51 | 13.40 |
| $\lambda$[Rh(3*d*), Rh] | 15.85 | 13.44 |
| $\lambda$[Rh(3*d*), $Rh_2O_3$] | 19.32 | 16.40 |
| $\lambda$[Au(4*f*), Rh] | 18.08 | 15.75 |
| $\lambda$[Au(4*f*), $Rh_2O_3$] | 22.06 | 19.20 |
| $\lambda$[Au(4*f*), Au] | 16.47 | 14.42 |

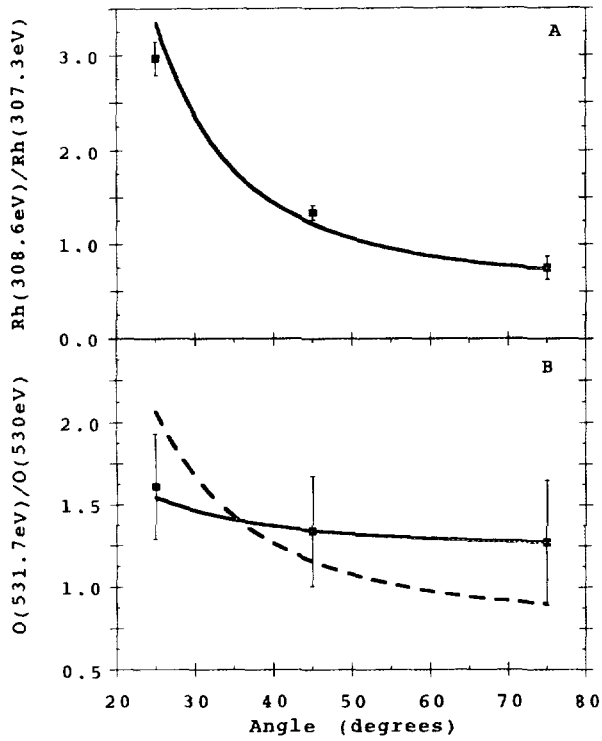


FIG. 10. Area ratios as a function of electron take-off angle for the polycrystalline rhodium foil. (A) Solid squares are Rh 308.6/307.3 experimental data and the solid line represents the calculated intensity ratio assuming a uniform oxide overlayer of thickness 14 Å. (B) Solid squares are O 531.7/530 experimental data. The dashed curve represents a model which assumes all 531.7-eV oxygen is chemisorbed on an oxide layer, and the solid line is a uniformly mixed oxide model with a monolayer of chemisorbed oxygen as shown in Fig. 11.

Rh film experiments, and a Mg source for the polycrystalline foil data, two sets of $\lambda_i$ values are included in Table 3.

Values of $\lambda_i$ for electrons traveling through either Rh or Au were calculated using material constants and parameters given in Ref. (44). For electrons traveling through $Rh_2O_3$, material constants, including the free-electron plasmon energy, density, molecular weight, and the number of valence electrons, were used to estimate the needed parameters. Finally, inelastic mean-free path values for adsorbed oxygen and oxygen associated with rhodium oxide were assumed to be equal.

Given the resulting $\lambda_i$ values, the curve-fitted $Rh^{3+}/Rh^0$ peak intensity ratio, and assuming a uniform overlayer model, we calculated the rhodium oxide layer thickness for the heavily oxidized Rh foil to be about 14 Å from the angle-dependent XPS data. The fit of the model to the $Rh^{3+}/Rh^0$ intensity ratio as a function of angle is shown in Fig. 10A, which confirms the plausibility of the layer model for this system. Assuming first that the 530-eV oxygen is associated with only the rhodium oxide and that the 531.7-eV peak is chemisorbed oxygen yields the dashed line in Fig. 10B to describe the angle dependence of the 531.7-eV/530-eV peak intensity ratios. The error bars in the oxygen ratio are considerably larger than for $Rh^{3+}/Rh^0$ because small variations in the curve fitting of the three peaks in the O(1*s*) envelope produce significant variations in the 531.7-eV vs 530-eV peak area ratio. Even though the dashed curve passes close to one standard deviation of the data points, it gives a value for the thickness of the chemisorbed layer of 6 Å, an unreasonably large value for a monolayer. Consequently, at least some of 531.7 eV oxygen must be present as a second type of oxide species. RhOOH or $RhO_2$ are the two most likely additional rhodium oxides. Inspection of the Rh(3*d*) spectra reveals relatively narrow linewidths, suggesting the presence of $Rh^{3+}$ exclusively, thereby supporting the assignment of the 531.7 eV oxygen to the oxyhydroxide because both RhOOH and $Rh_2O_3$ have a rhodium oxidation state of 3+.

If we assume that both oxygen atoms in either RhOOH or $RhO_2$ are chemically equivalent and contribute only to the O(1*s*) intensity at 531.7 eV, a layer model with $Rh_2O_3$ covered by the RhOOH/$RhO_2$, which, in turn, lies under a monolayer of chemisorbed oxygen, gives an angular dependence with a high curvature similar to that shown by the dashed line in Fig. 10B. To calculate the stoichiometries of $Rh_2O_3$ and RhOOH/$RhO_2$ predicted by the model, we need to know the detection efficiency factor for the spectrometer at O(1*s*) and Rh(3*d*) electron kinetic energies. In order to estimate these values, the Rh($3p_{1/2}$) and Rh($3d_{5/2,3/2}$) regions of a reduced rhodium foil were analyzed. Since the Rh($3p_{1/2}$) peak position at a binding energy of 522 eV is close to the O(1*s*) peak at ca. 530 eV, an accurate detection efficiency can be calculated from the measured intensities, the Scofield cross sections, and the mean-free paths. The value found was $D$(522 eV)/$D$(307 eV) = 1.25. This value yields a high O/Rh atomic ratio of 2.6 for RhOOH/$RhO_2$ layer. Furthermore, such a layer structure with RhOOH/$RhO_2$ covering $Rh_2O_3$ is unlikely to permit reduction of $Rh_2O_3$ and RhOOH/$RhO_2$ in parallel as shown in Fig. 7.

The surface model found to be most consistent with the angle-resolved XPS results is shown schematically in Fig. 11. This consists of a monolayer of oxygen adsorbed on top of a mixture of two chemically distinct rhodium oxides. The phases are separated in the drawing for clarity but are probably at least partly intermixed. The best fit to the ARXPS data (the solid curve in Fig. 10B) was obtained using a roughly equimolar mixture of $Rh_2O_3$ and either RhOOH or $RhO_2$, along with a monolayer of chemisorbed oxygen. We again assume that the oxygen atoms in either RhOOH and $RhO_2$ are equivalent and contribute only to the O(1*s*) intensity at 531.7 eV. Using the detection efficiency ratio described above along with the model in

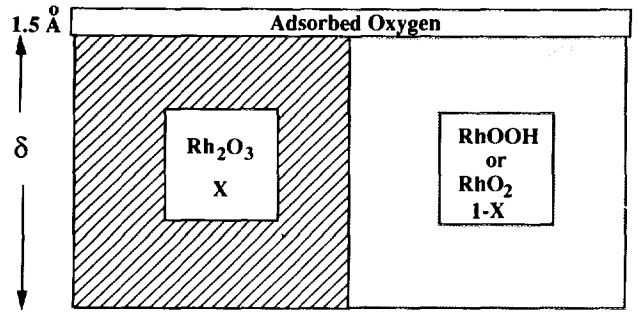


FIG. 11. Schematic representation of a proposed model for the oxidized rhodium surface. When $\delta = 14$ Å, $x = 0.5$. When $\delta = 8$ Å, $x = 0.67$.

Fig. 11 gave O/Rh atomic ratios of 1.7 and 2.1 for the $Rh_2O_3$ and RhOOH/$RhO_2$ oxides, respectively.

No reference XPS spectra for $RhO_2$ were found in the literature, so the core binding energy shifts for this compound are not available for comparison. The alternative oxide considered here, RhOOH, has been proposed primarily from XPS as the predominant species present on a heavily electrooxidized Rh surface (32). The observed presence of the O(1*s*) peak at 531.7 eV is consistent with the present XPS spectra. However, the inferred extensive formation of RhOOH would clearly require the involvement of hydrogen and/or water in the surface chemistry. While we certainly cannot eliminate this possibility, no clearcut evidence for surface hydroxyl groups was obtained from the infrared experiments described above.

A possible explanation for this additional oxygen species might seem to be oxygen adsorbed on nonreactive sites caused by structural changes in the film due to its exposure to high temperatures. STM micrographs of the rhodium film before and after oxidation did reveal that oxidation of the film caused the surface to break up into smaller roughness features. However, since the polycrystalline rhodium foil exhibited essentially identical oxidation–reduction behavior to the film, these structural changes are probably incidental to the observed chemical behavior.

The final O(1*s*) band to be assigned is the higher binding-energy peak, at 533.5 eV, which remains upon heating the Rh foil for extended periods above 200°C in UHV. Approximately half of the intensity of this feature might be ascribed to $SiO_2$ formed from Si impurities in the rhodium. The remainder may be due to "subsurface" oxygen, since its peak intensity increases noticeably toward higher (i.e., closer to normal) electron collection angles. The formation of subsurface oxygen, i.e., not being part of a discrete oxide lattice, has been proposed previously (6, 7, 14).

Utilizing the measured ratio of Rh(3*d*)/Au(4*f*) intensities for the fully oxidized rhodium film, and again assuming a uniform layer model, the rhodium oxide layer was deduced to be about 8 Å, or 3.5 monolayers, thick. This result is roughly compatible with the quantity of rhodium known to be present from the electrochemical deposition procedure. Similarly to the analysis for the rhodium foil, assuming all the oxygen responsible for the 531.7-eV peak is simply chemisorbed yields an overlayer thickness of ca. 4 Å, clearly too large to be compatible with that model. Although roughness of the film precludes angle-dependent analysis, we have used the flat surface model (Fig. 11), which provided a reasonable fit to the Rh foil data, to estimate the film composition. Combining the equivalent oxide layer thickness of 8 Å, obtained above, with the measured O(1*s*) 531.7 eV/530 eV peak intensity ratio yields a value of $X$, the fraction of pure $Rh_2O_3$, of two-thirds. Stoichiometries of the two oxides were determined in the same way as for the foil and gave values of 1.7 and 2.5 for the $Rh_2O_3$ and RhOOH/$RhO_2$ oxides, respectively. The value of 2.5 for the RhOOH/$RhO_2$ oxide stoichiometry is high, and would require additional 531.7 eV intensity to be associated with the chemisorbed oxygen. Since the film does break up into smaller features, a patchy surface model may be a better representation of the film surface than the uniform overlayer model. However, alternate models involving patches of oxidized rhodium (as might be expected in reality) and all but the most extreme cases of surface roughness still cannot account for all the oxygen associated with the 531.7-eV component in terms of a chemisorbed oxygen monolayer alone. We are therefore obliged again to invoke the presence of a significant additional oxide component other than $Rh_2O_3$.

The observed lower reactivity of CO with the species apparently responsible for the SERS feature at 290 $cm^{-1}$ and the XPS band at 531.7 eV, rather than the $Rh_2O_3$, may be rationalized by considering that the CO oxidation reaction on Rh surfaces is known to proceed via a Langmuir–Hinshelwood mechanism involving adsorbed CO (1–3). Rates for CO oxidation are found to be much lower on oxidized metal surfaces than on bare metals, presumably due to a lower sticking probability of CO on the former (1). Therefore, reaction of CO with either of the two oxides would require some metal adsorption sites which would become available only after the reduction of some $Rh_2O_3$. This idea is supported by the observation that attenuation of the Raman band at 290 $cm^{-1}$ begins only after some oxide is removed, as inferred by the decreasing 530 $cm^{-1}$ band intensity, and the emergence of adsorbed CO as manifested in a peak at 465 $cm^{-1}$, due to the Rh–CO stretch. Once adsorbed CO is formed extensively, the 290- as well as the 530-$cm^{-1}$ Raman band are seen to diminish in concert. The XPS data also exhibit qualitatively similar behavior, as shown in Fig. 7. Thus the XPS peak at 531.7 eV shows some initial resistance to reduction by CO, but once some $Rh_2O_3$ is removed,

both the 531.7- and 530-eV peaks lose intensity with increasing temperature.

The transient formation of the 290-$cm^{-1}$ SERS feature observed in route to the dominant production of the 530-$cm^{-1}$ band (Fig. 4) indicates that the former oxide can act as an intermediate state in forming $Rh_2O_3$. The ability of the 290-$cm^{-1}$ (and 531.7 eV) oxide species to form readily on ultrathin (<2 monolayer) rhodium films suggests that it does not require the three-dimensional lattice matrix required for the production of $Rh_2O_3$.

Finally, it is intriguing to note the spectral similarities in the thermal oxidation of rhodium films as studied here, with their *electrochemical* oxidation in aqueous environments (28), both studied by SERS. In the latter case, the formation of surface oxide is achieved at ambient temperatures by progressively increasing the electrode potential under voltammetric conditions whereupon water and/or hydroxide ion decomposition occurs. The spectral sequences obtained during such potential-induced rhodium oxidation in acidic media (28) feature SERS bands at 290 and ca. 530 $cm^{-1}$, which are strikingly similar to the spectra for the *thermally* induced rhodium oxide which is reported here.

## CONCLUDING REMARKS

We have presented a comprehensive study of the progressive oxidation of thin rhodium films deposited on gold substrates and polycrystalline Rh foil using SERS and XPS. The films were found to be chemically indistinguishable from polycrystalline rhodium foil, as indicated by the Rh(3*d*) binding energies. The SERS and XPS data show several different states of oxygen as indicated by Raman bands at 290, ca. 530, and 800 $cm^{-1}$, the two resolved O(1*s*) XPS peaks at 530 and 531.7 eV, and a peak at 533.5 eV on the oxidized Rh foil. The 530-eV peak is assigned to a stoichiometric $Rh_2O_3$ structure. The occurrence of $Rh_2O_3$ is supported by the presence of the Raman band at 530 $cm^{-1}$. The Raman assignment is based partly on a comparison with bulk–compound spectra and temperature and film-thickness dependencies of the spectra. The formation of a stoichiometric, perhaps even crystalline, oxide on a thin rhodium film, only 3–5 atomic layers thick, suggests that surface oxides contained in only a few atomic layers can take a form that is at least partially similar to that of bulk oxides.

Additional oxygen species other than $Rh_2O_3$ were also found on the oxidized rhodium surface. A spatial structural model for the different oxide species on the rhodium surface is proposed. The existence of an oxyhydroxide (RhOOH) or dioxide ($RhO_2$) along with adsorbed oxygen is suggested based on the XPS binding energies and their spatial distribution; however, no independent evidence for these species was found.

A final interesting conclusion that may be drawn from this study is that very *thin* rhodium films on gold substrates behave remarkably similarly to polycrystalline rhodium foils in terms of their oxidation–reduction behavior as well as the reactivity of their oxides toward CO. This is indeed a fortunate circumstance, since it supports the notion that SERS on thin transition-metal film provides information of direct relevance to actual catalysts. The above not only makes these films good model catalysts, but also may have implications for the design and manufacture of industrial rhodium catalysts.

## ACKNOWLEDGMENTS

We thank Christopher Panczyk for valuable assistance with the infrared experiments, Mary Crawford for undertaking the STM measurements, and Susan Peter for obtaining the scanning Auger data. This work is supported by NSF Grant CTS-9312008 (to CGT and MJW) and in the earlier stages by NSF Grant CHE-9119510 (to MJW).

## REFERENCES

1. Peden, C. H. F., Goodman, D. W., Blair, D. S., Berlowitz, P. J., Fisher, G. B., and Oh, S. H., *J. Phys. Chem.* **92,** 1563 (1988).
2. Oh, S-M., and Carpenter, J. E., *J. Catal.* **80,** 472 (1983).
3. Savchenko, V. I., Boreskov, G. K., Kalinkin, A. V., and Salanov, A. N., *React. Kinet. Catal.* **24,** 983 (1982).
4. Lee, C., and Schmidt, L. D., *J. Catal.* **101,** 123 (1986).
5. Gao, S., and Schmidt, L. D., *J. Catal.* **111,** 210 (1988).
6. Theil, P. A., Yates, J. A., and Weinberg, W. H., *Surf. Sci.* **82,** 22 (1979).
7. Castner, D. G., and Somorjai, G. A., *Appl. Surf. Sci.* **6,** 29 (1980).
8. Root, T. W., Schmidt, L. D., and Fisher, G. B., *Surf. Sci.* **134,** 30 (1983).
9. Logan, A. D., Datye, A. K., and Houston, J. E., *Surf. Sci.* **245,** 280 (1991).
10. Craig, J. H., and Lozano, J., *Appl. Surf. Sci.* **45,** 151 (1990).
11. Comelli, G., Dhanak., V. R., Kiskinova, M., Pangher, N., Paolucci, C., Prince, K. C., and Rosei, R., *Surf. Sci.* **260,** 7 (1992).
12. Bowker, M., Gou, Q., and Joyner, R., *Surf. Sci.* **53,** 33 (1991).
13. Castner, D. G., and Somorjai, G. A., *Surf. Sci.* **83,** 760 (1979).
14. Campbell, C. T., and White, J. M., *J. Catal.* **54,** 289 (1978).
15. Wong, C., and McCabe, R. W., *J. Catal.* **107,** 535 (1987).
16. Vis, J. C., van'T Blik, H. F. J., Huizinga, T., van Grondelle, J., and Prins, R., *J. Catal.* **95,** 333 (1985).
17. Ho, Y.-S., and Yeh, C.-Y., *Adsorpt. Sci. Technol.* **7,** 1 (1990).
18. Koshy, J., *Thin Solid Films* **51,** L17 (1978).
19. Pockrand, I., *Springer Tract in Modern Physics* **104,** 1 (1984).
20. Nowobiliski, P. J., Wilke, T., Davies, J. P., Patterson, M., Weaver, M. J., and Takoudis, C. G., "Proceedings, 9th International Congress on Catalysis, Calgary 1988" (M. J. Phillips and M. Ternan, Eds.). Chem. Institute of Canada, Ottawa, 1988.
21. McBreen, B. M., and Moskovits, M., *J. Catal.* **103,** 188 (1987).
22. Wilke, T. E., Gao, X., Takoudis, C. G., and Weaver, M. J., *Langmuir* **7,** 714 (1991).
23. Wilke, T. E., Gao, X., Takoudis, C. G., and Weaver, M. J., *J. Catal.* **130,** 62 (1991).
24. Tolia, A., Wilke, T., Weaver, M. J., and Takoudis, C. G., *Chem. Eng. Sci.* **47,** 2781 (1992).
25. Tolia, A., Weaver, M. J., and Takoudis, C. G., *J. Vac. Sci. Technol., A* **11,** 2013 (1993).

26. Leung, L.-W. H., and Weaver, M. J., *J. Am. Chem. Soc.* **109,** 5113 (1987).
27. Leung, L.-W. H., and Weaver, M. J., *Langmuir* **4,** 1076 (1988).
28. Zhang, Y., Gao, X., and Weaver, M. J., *J. Phys. Chem.* **97,** 8656 (1993).
29. Dubois, L. H., *J. Chem. Phys.* **77,** 5228 (1982).
30. Fisher, G. B., and Schmeig, S. J., *J. Vac. Sci. Technol., A* **1,** 1064 (1983).
31. Weber, W. H., Baird, R. J., and Graham, G. W., *J. Raman Spectrosc.* **19,** 239 (1988).
32. Peuckert, M., *Surf. Sci.* **141,** 500 (1984).
33. Huizinga, T., Van'T Blik, H. F. J., Vis, J. C., and Prins, R., *Surf. Sci.* **135,** 580 (1983).
34. Burkhardt, J., and Schmidt, L. D., *J. Catal.* **116,** 240 (1989).
35. Wang, T., and Schmidt, L. D., *J. Catal.* **71,** 411 (1981).
36. Gao, P., Gosztola, D., Leung, L-W. H., and Weaver, M. J., *J. Electroanal. Chem.* **233,** 211 (1987).
37. Doniach, S., and Sunjic, M., *J. Phys. C* **3,** 295 (1970).
38. Moskovits, M., *Rev. Mod. Phys.* **57,** 783 (1985).
39. Xie, Y., and Sherwood, P. M. A., *Chem. Mater.* **2,** 295 (1990).
40. Scofield, J. H., *J. Electron Spectrosc. Relat. Phenom.* **8,** 129 (1976).
41. Fadley, C. S., *J. Electron. Spectrosc. Relat. Phenom.* **5,** 725 (1974).
42. Fraser, W. R., Florio, J. V., Delgass, W. N., and Robertson, W. D., *Surf. Sci.* **36,** 661 (1973).
43. Griffith, W. P., *Coord. Chem. Rev.* **5,** 459 (1970).
44. Tanuma, S., Powell, C. J., and Penn, D. R., *Surf. and Interface Anal.* **11,** 577 (1988).